

See discussions, stats, and author profiles for this publication at: <https://www.researchgate.net/publication/263947461>

Experimental and Numerical Investigation on Soot Behavior of Soybean Biodiesel under Ambient Oxygen Dilution in Conventional and Low-Temperature Flames

ARTICLE *in* ENERGY & FUELS · APRIL 2014

Impact Factor: 2.79 · DOI: 10.1021/ef5002315

CITATIONS

7

READS

52

5 AUTHORS, INCLUDING:



Haifeng Liu

Tianjin University

48 PUBLICATIONS 1,012 CITATIONS

[SEE PROFILE](#)



Xiaojie Bi

Shanghai Jiao Tong University

5 PUBLICATIONS 54 CITATIONS

[SEE PROFILE](#)



Hu Wang

Tianjin University

25 PUBLICATIONS 243 CITATIONS

[SEE PROFILE](#)

Experimental and Numerical Investigation on Soot Behavior of Soybean Biodiesel under Ambient Oxygen Dilution in Conventional and Low-Temperature Flames

Maoyu Xiao,[†] Haifeng Liu,^{*,‡} Xiaojie Bi,[†] Hu Wang,[§] and Chia-fon F. Lee^{▽,⊥}

[†]Key Laboratory for Power Machinery and Engineering of Ministry of Education, Shanghai Jiao Tong University, Shanghai, 200240, People's Republic of China

[‡]State Key Laboratory of Engines, Tianjin University, Tianjin, 300072, People's Republic of China

[§]Engine Research Center, University of Wisconsin–Madison, Madison, Wisconsin, 53705, United States

[▽]Department of Mechanical Science and Engineering, University of Illinois at Urbana–Champaign, Urbana, Illinois, 61801, United States

[⊥]Center for Combustion Energy, Tsinghua University, Beijing 100084, People's Republic of China

ABSTRACT: Biodiesel is a type of particularly attractive alternative fuel for diesel engines. Many studies have investigated the combustion and emissions as fueling biodiesel on diesel engines and constant volume chambers. However, the understanding of the processes of biodiesel soot formation/oxidation is still limited. Therefore, in this work, high time-resolved quantitative soot measurements were carried out on a constant volume chamber by fueling soybean biodiesel. Three different ambient oxygen concentrations (21%, 16%, 10.5%) were tested at a conventional ambient temperature (1000 K) of diesel engine combustion and a lower ambient temperature (800 K). Results showed that the soot appearance was delayed at lower ambient temperatures and oxygen concentrations. At 800 K, less soot mass was observed with decreasing in oxygen concentration. However, soot mass increased with decreasing oxygen concentration as the ambient temperature reaching to 1000 K. To further illuminate the opposite trend on soot behavior in different temperature flames, a semiempirical biodiesel soot model was proposed and implemented into computational fluid dynamics (KIVA-3V, Release 2) code. Validation results showed that the proposed biodiesel soot model could successfully reproduce the entire process of soot formation and oxidation under various oxygen concentrations and ambient temperatures. With decreasing temperature, the appearance of intermediate species about soot formation/oxidation was delayed and the time-integrated mass of C_2H_2 , soot precursors, OH radicals, and soot was reduced. The soot formation mechanism dominated soot evolution and caused a lower soot mass as the ambient temperature decreased. The formation of soot precursors presented a stronger temperature dependence than biodiesel pyrolysis. Regardless of whether the initial ambient temperature was 800 K or 1000 K, soot oxidation was significantly suppressed as the ambient oxygen concentration was reduced. However, the temperature did change the evolutionary tendency of soot formation with decreasing ambient oxygen concentrations. At 800 K, the time-integrated mass of acetylene and soot precursors and the regions of high equivalence ratios were reduced as the ambient oxygen concentration decreased; therefore, the soot formation was inhibited effectively at lower oxygen concentrations. At 1000 K, the time-integrated mass of acetylene and soot precursors and the regions of high equivalence ratios increased with the decrease of ambient oxygen concentration; therefore, the soot formation was motivated at lower oxygen concentrations. It can be concluded that soot formation transition was the responsible factor for the nonconsistent soot behavior, because of ambient oxygen dilution in conventional and low-temperature flames.

1. INTRODUCTION

The dependency on fossil fuels has caused a series of critical social issues, such as energy supply crisis, climate change, and threats to human health. For example, the carbon dioxide emissions that have been ascribed to the combustion of fossil fuels are capable of substantially harming the worldwide ecosystems.¹ The particulate matter (PM) emissions from gasoline direct injection (GDI) engines and diesel engines, especially those PM2.5 particles (diameter of $<2.5\text{ }\mu\text{m}$) are directly associated with lung disease.² The continuous growth of energy demand, together with the depletion of fossil fuel reserves, has led to serious geopolitical and military conflicts.³ These problems indicate an unsustainable future of sole fossil fuel supply. Therefore, the development of renewable energy is

the motivation behind solving the increasing challenges regarding energy and environment.

Biodiesel is one of the particularly attractive alternative fuels, because of its renewability and sustainability,^{4–6} and it can be derived from renewable vegetable oils, algae, and waste cooking oil.^{7,8} Biodiesel can be directly used in current diesel engines without too much modification. Furthermore, the current diesel fuel infrastructure is compatible to biodiesel fuel. Based on comparative experiments in diesel engines, the biodiesel-fueled engine indicates that biodiesel has similar combustion characteristics to diesel fuel and the power outputs to these

Received: January 24, 2014

Revised: March 26, 2014

Published: March 26, 2014



two fuels are almost the same.^{9–12} As an alternative biofuel, biodiesel can mitigate CO₂ emissions due to the fact that CO₂ can be consumed in the growth of feedstocks during the manufacture of biodiesel.¹

Because biodiesel is blended into diesel fuel, it can reduce PM or soot emissions in diesel engines, because of the ~10% (by weight) oxygen content in biodiesel. Some previous studies have shown that soot emissions can be reduced steadily with the increase of biodiesel fractions in blending fuels.^{13–21} Although biodiesel is capable to provide the benefit of soot emissions, the application of biodiesel usually leads to the increase of NO_x emissions.^{20–23} Most literatures show that combining exhaust gas recirculation (EGR) and biodiesel is an effective method to decrease both NO_x and soot emissions simultaneously.^{23–28} The EGR can reduce NO_x emissions by controlling oxygen concentration and combustion temperature. However, the effects of EGR on soot emissions are very complicated. At low or medium EGR rate, the changes of soot emissions are very small. Then, the soot emission manifests a rapid increase with the EGR rate increasing further. Finally, over the peak value of soot emissions, the soot begins to reduce sharply with EGR rates continuing to increasing. Therefore, with the high EGR dilution, the low NO_x and soot emissions can be achieved simultaneously. In this low NO_x and soot regions, the combustion process is called as EGR dilution low temperature combustion, which has been seen as one of future advanced combustion modes for diesel engines to achieve high efficiency and clean combustion. Therefore, the study on the complicated effects of EGR on soot reduction mechanism is very crucial to reduce soot emissions and achieve the control on low temperature combustion process in diesel engines.

Kinetic modeling is well-known to be effective to gain in-depth knowledge about the chemical pathways leading to soot emissions. At present, the common practice in biodiesel model developing is the use of simpler surrogate molecules to replace the real fuel. In the early time, the kinetic model of short chain methyl ester such as methyl butanoate (C₅H₁₀O₂) was proposed by Fisher et al.²⁹ in 2000. With the further development on models, the kinetic models of longer chain methyl ester have been proposed in recent several years, such as methyl hexanoate (C₇H₁₄O₂),³⁰ methyl decanoate (C₁₁H₂₂O₂).³¹ Recently, chemical kinetics model for much longer chain methyl esters (C₁₁ to C₁₉) have been proposed by Herbinet et al.³² However, these kinetic models especially for low carbon molecular structures can not fully represent the combustion characteristics of real biodiesel. Also, as the detailed kinetic mechanisms usually include thousands of reactions, which are impractical to be used in simulation of diesel engines according to the current computational ability because the diesel combustion is complicated comprehensive processes including multiphase, turbulence, thermochemistry. Finally, it should be noted that the kinetic models are proposed under the fully premixed conditions. These models should be suitable to the homogeneous combustion in engines, such as the homogeneous charge compression ignition (HCCI). However, the diesel combustion is dominated by the diffusion flame in many operating conditions and the mixing process is very important to the diesel combustion. Therefore, the pure kinetic process may not reveal the processes of combustion and emissions in diesel engines.

Compared to kinetic models, semiempirical model is another essential kind of models to do multidimensional simulation. For example, Hiroyasu-NSC soot model³³ has significant contribu-

tions to understand of soot formation and oxidation and in hence to optimize the engine control strategies and performance. With simplified chemical reactions, the semiempirical soot model is able to be coupled into computational fluid dynamics (CFD) codes to simulate diesel combustion and soot emissions with high time efficiency. Someone may doubt that semiempirical soot model is too simplified to represent soot evolution in diesel combustion flame. Factually, soot formation/oxidation process is very complex and contains sophisticated chemical kinetics and particle dynamics, so its relevant descriptions are limited, especially for gas-phase kinetics from biodiesel to soot nuclei.³⁴ Detailed chemical kinetic soot models are believed to be more accurate because it includes more detailed description about chemical reactions and intermediate species. However, this detailed representation is required to simulate the interactions between the turbulent mixing and detailed chemistry on a subgrid level. Therefore, the detailed chemical kinetic soot model demands a quite long computation time and thus is rather impractical. Additionally, the precise predictions of soot formation/oxidation are also depending on other models such as spray, evaporation, turbulence model, etc. The present nondeterminacy in other models has weakened the benefits of a detailed kinetic mechanism for soot formation/oxidation. On the basis of the advantage on computation efficiency together with acceptable accurate, it is necessary to propose a semiempirical soot model aiming to biodiesel. In previous studies, semiempirical soot models of diesel fuel have been proposed in some literatures,^{35–37} but there is little report on the biodiesel semiempirical soot model to author's knowledge.

For the experimental studies of biodiesel, some literatures have explored the effects of different biodiesel blending ratios on combustion and emissions, but these studies are usually carried out on engine benches and focus on engine performance rather than on the fundamental aspects such as the spray, flame development and soot distribution. The effects of in-cylinder gas dilution and temperature on combustion and soot formation are very difficult to be isolated and to be solely studied based only on engine tests. The constant volume chamber is often applied to form well-characterized ambient environment for diesel spray combustion and has also been used for biodiesel research in a number of studies.^{5,11,16,18,38} Meanwhile, some optical diagnostic methods such as two color thermometry and laser-induced incandescence (LII) have been used to measure the biodiesel soot formation/oxidation process in previous studies.^{5,11,16,18,38} However, soot emissions are not directly measured in a burning spray plume by using two-color thermometry, while LII yields low temporal resolutions even though LII can provide the quantitative soot diagnostics. In this respective, quantitative high time-resolved soot measurement is a valuable supplement to the current knowledge base on biodiesel combustion.

Based on literature reviews, it can be found that the understanding on the biodiesel soot formation/oxidation is still limited based on advanced laser diagnostics and numerical models. Therefore, high time-resolved quantitative soot measurements were carried out on a constant volume chamber by the method of forward illumination light extinction (FILE)³⁹ and fueling soybean biodiesel. Three different ambient oxygen concentrations (21%, 16%, 10.5%) were tested at a conventional ambient temperature (1000 K) of diesel engines and a lower ambient temperature (800 K). Meanwhile, to further illuminate the different trends on soot behavior in conventional

and low-temperature flames, a semiempirical biodiesel soot model was proposed and coupled into computational fluid dynamics (KIVA-3V Release 2) code. Furthermore, the proposed semiempirical biodiesel soot model was validated by the measured soot results on the whole process of soot formation and oxidation. Detailed analysis of combustion pressure, heat release rate, time related traces and spatial distributions of soot formation/oxidation was provided to expand the understanding about coupled dependence of temperature, oxygen concentrations and soot nuclei.

2. EXPERIMENTAL APPARATUS AND METHODS

Experiments were carried out on a constant volume chamber, and the bore and height is 110 mm and 65 mm, respectively. An injector (Caterpillar Corp.) with 6 holes and 0.145 mm orifice diameter was used. The injection pressure was controlled at 134 MPa and the fuel flow-rate was 120 mm³ per injection to mimic a high engine load condition. The temperature of chamber wall was maintained 380 K. A pressure transducer (Kistler Corp., Model 6121) was mounted in the chamber wall for recording the combustion pressure. The detailed setup of constant volume chamber can be found in previous studies.^{40,41}

Generally, the in-cylinder temperature and density can reach 1000 K and 14.8 kg/m³ at top dead center in diesel engines without EGR dilution (21% oxygen concentration). To simulate the different thermodynamic conditions in conventional and low temperature combustion (LTC) modes when the fuel injection occurs, the ambient temperatures were controlled at 1000 and 800 K in this work. The ambient oxygen concentrations were controlled at 21%, 16%, and 10.5% to mimic no EGR, medium EGR and high EGR levels in diesel engines. The ambient density was set to 14.8 kg/m³. The ambient temperature and ambient oxygen concentration was defined here as the in-chamber temperature and oxygen concentration at the start of fuel injection. Biodiesel fuel was bought from Incobrasa Industries Ltd. in United States and fuel properties were listed in Table 1. More detailed fuel properties can be found in previous studies.^{41,42}

Table 1. Fuel Properties of Soybean Biodiesel

property	value
density @15 °C [g/cm ³]	0.887 (D1298) ^a
viscosity @40 °C [mm ² /s]	4.0 (D445)
cetane number	51 (D613)
sulfur [ppm]	<1 (D5453)
mMidboiling point [°C]	329.7 (D1160)
lower heating value [MJ/kg]	37.53 (D240)
latent heating @ 25 °C [kJ/kg]	200
stoichiometric air-fuel ratio	12.5
oxygen content [wt %]	10

^aAll test methods are the American Society for Testing and Materials (ASTM).

Forward illumination light extinction method³⁹ was adopted in this study to present high time-resolved quantitative soot measurement. The FILE method had been implemented in a constant volume chamber to investigate the spray, combustion, and soot formation/oxidation by using diesel and some alternative fuels.^{40–45} The current incident light for soot measure was provided by a copper vapor laser (Oxford Lasers Corp., Model LS20–50) and the repetitive frequency of laser pulse can cover from 4.5 kHz to 20 kHz and each pulse can last 25–30 ns. A high-speed camera (Phantom Corp., Model V7.1) equipped with a 105 mm focal length lens (Nikon) was used to take the light signal. The laser and the camera were synchronized up to 15 037 frames per second at resolution of 256 × 256 pixels. The detailed setup for the soot measurement can be found in previous studies.^{41,42}

3. THE NUMERICAL MODELS

3.1. Semiempirical Biodiesel Soot Model. In order to illuminate the soot behavior in diesel combustion flames with different temperatures and oxygen concentrations, a semiempirical biodiesel soot model was proposed. The schematic diagram of the semiempirical biodiesel soot model is illustrated in Figure 1. There were mainly nine steps reaction in the soot

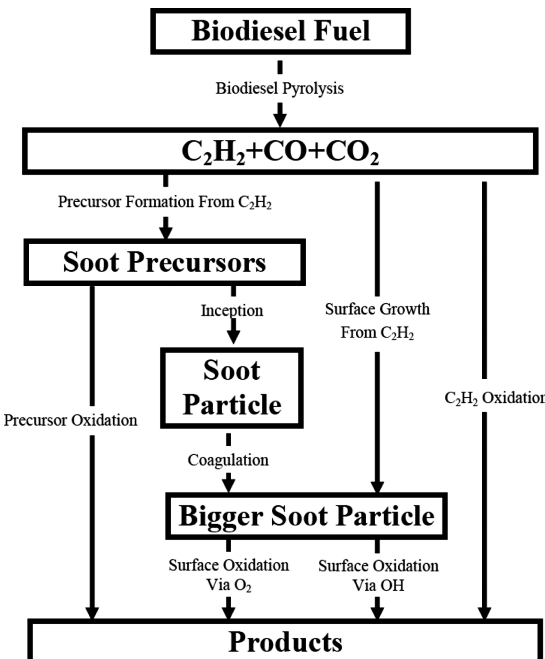
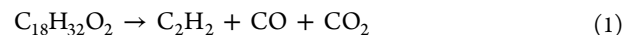


Figure 1. Schematic of semiempirical biodiesel soot model.

model to express the soot formation and oxidation processes. To save the computational time, the chemical reactions in proposed soot model were simplified by one-step global reaction, which was similar to the previous studies.^{35–37} Detailed descriptions for the semiempirical biodiesel soot model are shown as follows.

Step 1: Biodiesel Pyrolysis. For conventional diesel fuel, it is composed of hundreds of compounds, including paraffins, cycloparaffins, aromatics, etc. However, for biodiesel fuel derived from soybeans, it mainly contains five long-chain C₁₆ and C₁₈ saturated and unsaturated methyl esters, as reviewed in previous study.²⁹ Since methyl linoleate (C₁₈H₃₂O₂) has the largest fractions in soybean biodiesel, it was used to be the surrogate of biodiesel in the proposed model. The chemical reaction and reaction rate for biodiesel pyrolysis are expressed as eqs 1 and 2, respectively.



$$\omega_1 = 3.0 \times 10^9 \exp\left(\frac{-2.5 \times 10^4}{T}\right) \times [\text{C}_{18}\text{H}_{32}\text{O}_2] \quad (2)$$

Unlike the conventional diesel pyrolysis, some previous studies have shown that the pyrolysis reaction of methyl esters group can directly generate CO and CO₂.^{46–50} Szybist et al.⁴⁸ has reported that ~6%–9% of fuel carbon was converted to CO₂ during low-temperature heat release (LTHR), using methyl decanoate on a motorized engine. Dagaut et al.⁴⁹ has measured CO₂ in jet stirred reactor experiments, using rapeseed oil methyl ester as fuel. Chemical kinetics studies of methyl

ester groups have shown that CO₂ formation is significant in the low-temperature reaction region.⁵⁰ In other words, the CO and CO₂ are formed before any significant heat release has been detected. The oxidation of CO into CO₂ did not occur during LTHR as hydrocarbon fuel was present. Therefore, the detected CO₂ in LTHR indicates that decarboxylation of ester groups occurs during LTHR. Therefore, the formation of CO and CO₂ was taken into account in biodiesel pyrolysis.

According to the previous studies,⁵¹ the energy barrier of the CO₂ reaction is ~14.7 kcal/mol, whereas the barrier of the CO reaction is >22 kcal/mol. Therefore, CO₂ formation should be the primary reaction pathway, because of its lower energy barrier in biodiesel pyrolysis. Accordingly, the mole ratio of CO₂ and CO was assumed to be 3:2 in the biodiesel pyrolysis process, based on the ratios of the barrier of reaction channels. Although acetylene (C₂H₂) is not the sole hydrocarbon fragment during biodiesel pyrolysis, it has been widely considered to be the primary species in pyrolysis. To improve the computational efficiency for the proposed model, C₂H₂ was considered to be the only product in the biodiesel pyrolysis process and other hydrocarbon species were formed from the C₂H₂ pool in the current model.

Step 2: Formation of Soot Precursors (P). The chemical reaction and reaction rate for soot precursors (P) is expressed as eqs 3 and 4, respectively. The formation of soot precursors was simplified to a one-step reaction, instead of detailed kinetic reactions of polycyclic aromatic hydrocarbons (PAHs). In the current model, soot precursors were considered as the common gaseous precursors and were defined as fullerene consisting of 60 C atoms with a ball structure.



$$\omega_2 = 1.0 \times 10^{10} \exp\left(\frac{-2.0 \times 10^4}{T}\right) \times [\text{C}_2\text{H}_2] \quad (4)$$

There are some reasons to support the above assumptions. First, the chemical kinetic reactions involved in the formation of soot precursors are still uncertain.³⁴ The previous studies on the gas-phase kinetics of soot precursors have been primarily focused on the first benzene ring formation, since it is believed to be the basis for the formation of larger PAHs.^{52,53} The chemical pathways from the formation of larger PAHs to the initial soot nuclei are still uncertain and only a few of these phenomena have been detected and established. Therefore, simplified models with only small PAHs (up to four rings) are the most-popular applications in the diffusion-dominant combustion simulations.^{54–56} However, some recent soot investigations have shown that the heavier PAHs with seven rings are observed, so it should be more reasonable to accept that the reactions of initial soot nuclei should come from heavier PAHs with seven rings.^{57,58} Moreover, the absence of heavier PAHs has resulted in a considerable predicted error in soot mass, which is reported as high as 50% in the simulation results.³⁴ In addition, as the detailed kinetics of PAH formations are coupled into CFD model, the interactions between turbulent mixing and detailed chemistry must be solved on a subgrid level. However, the model will be rather impractical to simulate the complicated diesel combustion with multiphase, turbulent, and thermochemical processes. Consequently, only a one-step global reaction was applied in the current model.

Step 3: Soot Inception Reaction. The chemical reaction and reaction rate for soot nuclei (S) are expressed as eqs 5 and 6, respectively, which demonstrates the soot nuclei process from soot precursors to nuclei. In the current work, the incipient soot nuclei were assumed to be pure dry carbon particles with the graphite-like structure and one soot nucleus was composed of 100 C atoms, as observed in the previous study.³⁶ Although a large amount of hydrogen has been observed in young soot nuclei, the fraction of hydrogen in soot nuclei will decrease as the soot changes mature.⁵¹ Furthermore, the final composition in soot is not quite clear. Therefore, the assumption of dry carbon particles should be acceptable, given the lack of a better alternative.



$$\omega_3 = 1.0 \times 10^7 \exp\left(\frac{-2.52 \times 10^4}{T}\right) \times [\mathbf{P}] \quad (6)$$

Step 4: Soot Particle Coagulation. The particle coagulation and reaction rate are expressed as eqs 7 and 8, respectively, which demonstrates the soot coagulation process from small nuclei to some bigger particles. Therefore, in eq 7, the value of x should be larger than 2. In the reaction rate of soot coagulation, k_4 is the collision frequency constant and N_s indicates the soot number density.



$$\omega_4 = \frac{1}{2} k_4 N_s^2 \quad (8)$$

The collision frequency constant (k_4) is defined as eq 9, according to ref 59, and k_4 can be used for both the free-molecular and near-continuum regimes.

$$k_4 = \frac{k_{\text{fm}} \times k_{\text{nc}}}{k_{\text{fm}} + k_{\text{nc}}} \quad (9)$$

The collision frequency (k_{fm}) is expressed as eqs 10 and 11 in the free-molecular regime,

$$k_{\text{fm}} = 4\alpha \sqrt{\frac{6k_B T d_p}{\rho_s}} \quad (10)$$

$$d_p = \left(\frac{6\text{MW}_c y_s}{\pi N \rho_s} \right)^{1/3} \quad (11)$$

where α is van der Waals enhancement factor, k_B the Boltzmann constant, d_p the mean diameter of soot nuclei, T the ambient temperature, ρ_s the soot nuclei density, MW_c the molecular weight of the C atom, and y_s the molar concentration of soot. For the soot mass density, it is chosen as $\rho_s = 2.0 \text{ g/cm}^3$, according to the investigations in refs 60 and 61.

The collision frequency (k_{nc}) is expressed as eqs 12 and 13 in the near-continuum regime,

$$k_{\text{nc}} = \frac{8k_B T}{\mu} (1 + 1.257k_n) \quad (12)$$

$$Kn = \frac{2l}{d_p} \quad (13)$$

where Kn is the Knudsen number, μ the gas viscosity, and l the gas mean free path.

Step 5: Surface Growth. It is well-accepted that gas-phase agents of surface growth are small hydrocarbon fragments and most likely to be acetylene. Therefore, the surface growth of soot particles is expressed as eq 14 and the reaction rate is expressed as eq 15, where A_s is the total surface area of soot nuclei. Previously, the reaction rate of surface growth was set to be a first-order approximation to acetylene concentration and total surface area of soot particles. However, this linear correlation exaggerated the effects of surface area, because of the insufficient amount of surface area, thus reducing the reactivity of the active surface. Therefore, the reaction rate of surface growth in this paper was assumed to be proportional to the square root of total surface area, as suggested by Leung et al.⁶²



$$\omega_5 = 1.05 \times 10^4 \exp\left(\frac{-3.1 \times 10^3}{T}\right) \times [C_2H_2] \times A_s^{1/2} \quad (15)$$

Step 6: O_2 -Related Surface Oxidation. The surface oxidation caused by oxygen and reaction rate is expressed as

$$[OH] = \frac{k_1^+[H][O_2] + k_2^+[O][H_2] + k_3^-[H_2O][H] + k_4^+[O][H_2O] + k_5^+[H_2O][M] + k_6^-[CO_2][H]}{k_1^-[O] + k_2^-[H] + k_3^-[H_2] + k_4^-[OH] + k_5^-[H][M] + k_6^+[CO]} \quad (20)$$

$$[M] = \frac{P}{RT} \quad (21)$$

where k_i^+ and k_i^- is forward and backward reaction rate constants of each reaction and the subscript i represents the different numbers from 1 to 6, M is third-body species. Detailed chemical mechanisms for the OH calculation have been shown in Table 2.

Table 2. Chemical Mechanisms for the OH Calculation³⁶

No.	reaction	A	K_f	
			b	E [cal/mol]
1	$H + O_2 \leftrightarrow O + OH$	1.915×10^{14}	0.00	1.644×10^4
2	$O + H_2 \leftrightarrow OH + H$	5.080×10^4	2.67	6.292×10^3
3	$OH + H_2 \leftrightarrow H_2O + H$	2.160×10^8	1.51	3.430×10^3
4	$O + H_2O \leftrightarrow OH + OH$	2.970×10^6	2.02	1.340×10^4
5	$H_2O + M \leftrightarrow H + OH + M$	1.912×10^{23}	-1.83	1.185×10^5
6	$CO + OH \leftrightarrow CO_2 + H$	9.430×10^3	2.25	-2.351×10^3

Step 8: Acetylene Oxidation. As reviewed in ref 64, soot oxidation can occur at any time between fuel pyrolysis to soot nuclei agglomeration. Therefore, besides soot particle oxidation, oxidation processes of acetylene and soot precursors have also been considered in the model described in Steps 8 and 9, as shown in eqs 22–25.



$$\omega_8 = 6.0 \times 10^{12} \exp\left(\frac{-2.52 \times 10^4}{T}\right) \times [C_2H_2] \times [O_2] \quad (23)$$

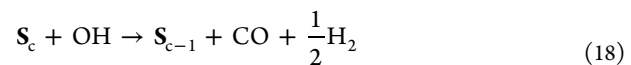


eqs 16 and 17, respectively, where k_6 is the oxidation rate constant derived from the Nagle–Stickland–Constable (NSC) oxidation model and the detailed introduction can be seen in ref 33.



$$\omega_6 = k_6 [O_2] A_s \quad (17)$$

Step 7: OH-Related Surface Oxidation. The surface oxidation caused by OH, and the corresponding reaction rate, are expressed as eqs 18 and 19, respectively, where k_7 is oxidation rate constant derived from Neoh's OH oxidation model and the detailed introduction can be seen in ref 63.



$$\omega_7 = k_7 [OH] A_s \quad (19)$$

The concentration of OH radical is obtained by using a quasi-steady state assumption based on a $H_2-O_2-CO_2$ system, as shown in eqs 20 and 21, respectively:

$$[OH] = \frac{k_1^+[H][O_2] + k_2^+[O][H_2] + k_3^-[H_2O][H] + k_4^+[O][H_2O] + k_5^+[H_2O][M] + k_6^-[CO_2][H]}{k_1^-[O] + k_2^-[H] + k_3^-[H_2] + k_4^-[OH] + k_5^-[H][M] + k_6^+[CO]} \quad (20)$$

$$[OH] = 1.0 \times 10^9 \exp\left(\frac{-2.0 \times 10^4}{T}\right) \times [P] \times [OH] \quad (25)$$

Step 9: Oxidation of Soot Precursors (P). Based on the above 9 steps, it can be found that all reactions can be divided into gas-phase reactions (including Steps 1, 2, 8, 9) and particle-related reactions (including Steps 3–7). The mass and mole concentration of soot particle are calculated in eqs 26 and 27, respectively.

$$\frac{d(m_s)}{dt} = MW_c(\omega_3 + \omega_5 - \omega_6 - \omega_7) \quad (26)$$

$$\frac{d(y_s)}{dt} = \omega_3 - \omega_4 \quad (27)$$

3.2. Computational Fluid Dynamics Models. In the current work, the computational fluid dynamics (KIVA-3V Release 2) was used to calculate the momentum, mass, and energy conservation equations in the biodiesel combustion process. The “blob” model was used to simulate the spray injection dynamics⁶⁵ and the Kelvin–Helmholtz and Rayleigh–Taylor model was applied to simulate the spray atomization and droplet break-up.^{66,67} The RNG $k-\epsilon$ model⁶⁸ was used to simulate the effects of turbulent motions on low Mach-number flow characteristics. The ignition was simulated by the Shell model and the combustion was simulated by the laminar-and-turbulent characteristic time combustion (CTC) model.⁶⁹ Considering the computation efficiency, a 60° sector mesh was selected in the study to present a single spray from one of six holes of the injector located in the center of constant volume chamber, as illustrated in Figure 2.

4. RESULTS AND DISCUSSION

4.1. Combustion and Soot Validation and Analysis.

Figure 3 presents the comparison of predicted in-chamber

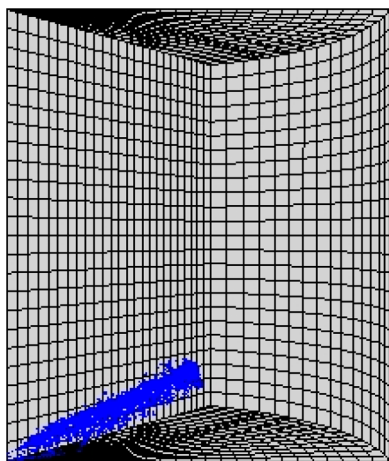


Figure 2. Mesh of the tested constant volume chamber.

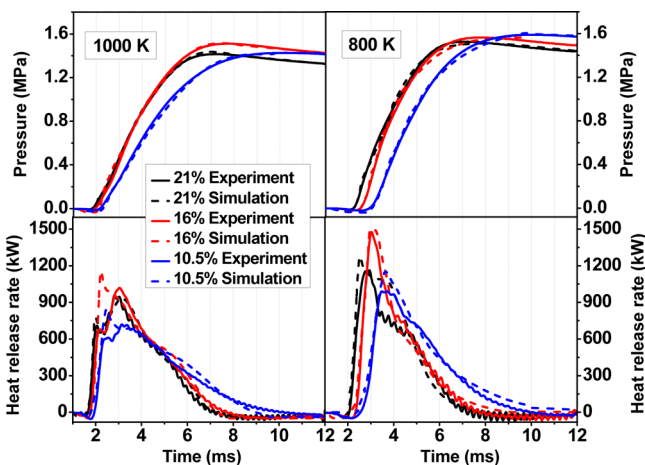


Figure 3. Comparison of predicted in-chamber pressure and heat release rate with experimental data under various ambient oxygen concentrations and temperatures.

pressure and heat release rate with experimental results under various oxygen concentrations in conventional and low-temperature conditions. It shows that the predicted chamber pressure and heat release rate has good agreement with the experimental results. As shown in Figure 3, the ignition delay became longer as the ambient temperature was reduced from 1000 K to 800 K or the ambient oxygen was diluted. The start of combustion was defined as the time of rapid increase in the heat release rate. Based on the theory of chemical kinetics, both the decrease of ambient temperature and oxygen concentration will result in less effective coagulation between reactants, and, hence, the chemical reaction rate will be slowed. Therefore, more time should be needed to achieve an autoignition at lower initial ambient temperature or ambient oxygen concentration, so the ignition delay is longer. At the 800 K condition, a longer autoignition delay made more ambient air enter into the biodiesel fuel jet and a greater amount of biodiesel and air mixture tended to burn in premixed combustion mode. The heat release rate in Figure 3 illustrated a transition from diffusion-dominated combustion at 1000 K to premix-dominated combustion at 800 K. Although ignition delay was also retarded with decreasing ambient oxygen concentration, no significant transition tendency was observed in the heat release

rate as the ambient oxygen concentration decreased from 21% to 10.5%.

Figure 4 illustrates the comparison between experimental and predicted soot using a semiempirical soot model under various

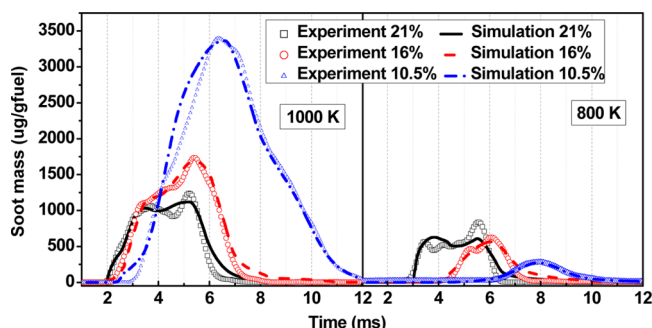


Figure 4. Comparison of predicted soot mass with experimental data under various ambient oxygen concentrations and temperatures.

ambient oxygen concentrations in conventional and low-temperature conditions. It can be seen that the overall predicted soot traces were in good agreement with experimental results. The FILE method provided a high time-resolved quantitative measurement on soot formation and oxidation process. The proposed soot model can reproduce the soot evolution during combustion. The previous studies of soot models mainly focused on the engine bench test, and the validation of soot model mainly came from the results of engine-out soot emissions.^{36,37,70,71} Therefore, the previous validations are aiming to the single value of soot emission. To the knowledge of the authors, there is little validation of soot models over the entire process of soot formation and oxidation, while the validation of soot evolution is very necessary to further analyze the soot behavior. As shown in Figure 4, soot mass concentration began to increase first, reached peak values, and then started to decrease after the peaks were attained. The start of soot formation was delayed as the ambient temperature reduced from 1000 K to 800 K or ambient oxygen concentrations decreased from 21% to 10.5%. As the above discussion, the autoignition was delayed as the ambient temperature and ambient oxygen concentration were reduced. Since soot particles are the incomplete products of combustion, they followed the similar characteristics of combustion and the occurrence of soot was also delayed with the decrease of ambient temperature and oxygen concentration.

Figure 5 shows the normalized time-integrated soot mass (NTISM) under various initial temperatures and ambient oxygen concentrations. The time-integrated soot mass was introduced because it considered not only the soot amount, but also the soot existing time within the flame. All of time-integrated total soot mass was normalized by the soot emission at 800 K and 21% ambient oxygen for a better comparison. The NTISM demonstrated the soot emission tendency in the exhaust pipe of diesel engines, and a higher NTISM value means a higher soot emission. As shown in Figure 5, biodiesel demonstrated larger soot tendency at an initial ambient temperature of 1000 K. The higher ambient temperature resulted in the shorter flame lift-off, which made less ambient air entrained into the spray jet and formed more fuel-rich regions. Therefore, soot formation rate was accelerated at the early stage of combustion and the total soot mass concentration increased with increasing of ambient temperatures. As ambient

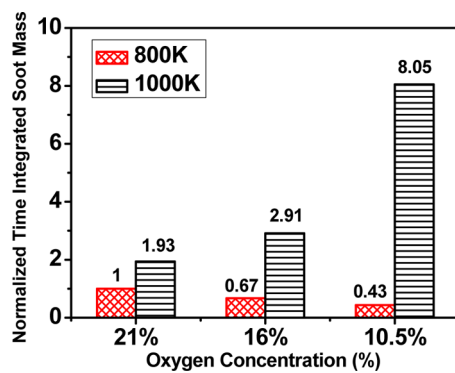


Figure 5. Predicted normalized time-integrated soot mass (NTISM) under various ambient temperatures and oxygen concentrations.

oxygen concentration decreased, soot behavior exhibited the opposite tendency in conventional and low-temperature flames. At an initial ambient temperature of 800 K, NTISM decreased with reducing ambient oxygen concentrations. However, at an initial ambient temperature of 1000 K, NTISM increased as the ambient oxygen concentrations were reduced.

Based on the above validation on combustion and soot, it can be found that the proposed biodiesel soot model successfully reproduces effects of oxygen concentrations and temperature on soot evolution. Therefore, in order to detailed and in-depth interpret the responsible factor for the nonconsistent variation caused by ambient oxygen reduction, the semiempirical biodiesel model has been employed to investigate the behavior of soot relevant intermediate reactants and get an insight into the formation and oxidation mechanisms of soot nuclei with various ambient oxygen dilutions in conventional and low-temperature conditions.

4.2. Predicted Traces of Intermediate Species on Soot Evolution

Figures 6 and 7 show the predicted temporal mass concentrations of C_2H_2 , soot precursors and OH radical, and soot number density. As shown in Figures 6 and 7, all temporal traces of intermediate species shared the similar “bell-shaped” characteristics and the thresholds for soot relevant species and soot number density were retarded with the decreasing in ambient temperature or ambient oxygen. A lower ambient temperature or oxygen concentration resulted in the reduction of chemical reaction rates in the entire combustion process. Therefore, the formation timing of soot formation/oxidation intermediate species such as acetylene, soot precursors, and OH radical were delayed.

Figure 8 presents the normalized time integrated mass of C_2H_2 , soot precursors, OH radical, and the normalized time-integrated soot number density. For constant ambient oxygen concentration, an obvious decrease in the time-integrated mass of C_2H_2 , soot precursors, and OH radical were observed as the initial ambient temperature decreased. It is well-accepted that the chemical reaction rates are proportional to ambient temperature and reactants' concentration, so a reduction in any of these two factors will directly lead to a slower rates for all chemical reactions involving in soot formation and oxidation. At 800 K, the formation reactions of C_2H_2 , soot precursors, and OH radical were inhibited because of the lower combustion temperature caused by the lower ambient temperature, as presented in Figure 7. Consequently, soot formation reactions based on acetylene and soot precursors as well as soot oxidation reactions dependent on OH radical were strongly suppressed simultaneously. Based on the result of competition between soot formation and oxidation, the time-integrated soot mass was decreased under lower ambient temperature, as shown in Figure 5. This indicated that soot formation mechanism

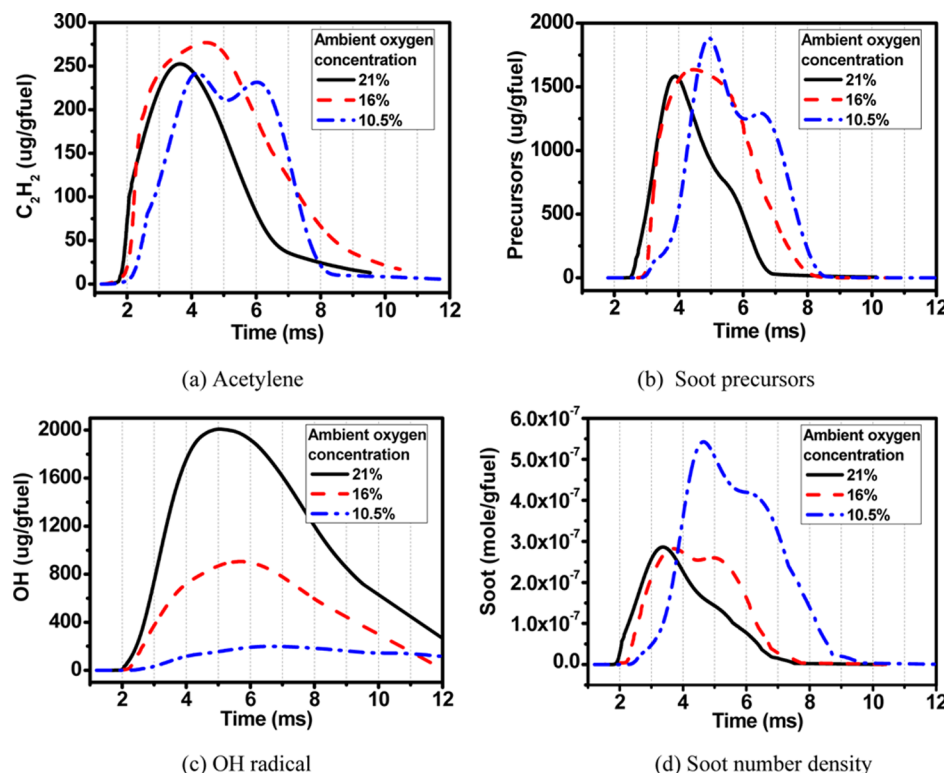


Figure 6. Effects of ambient oxygen concentrations on the concentrations of C_2H_2 , precursors, and OH radical, and soot number density at 1000 K.

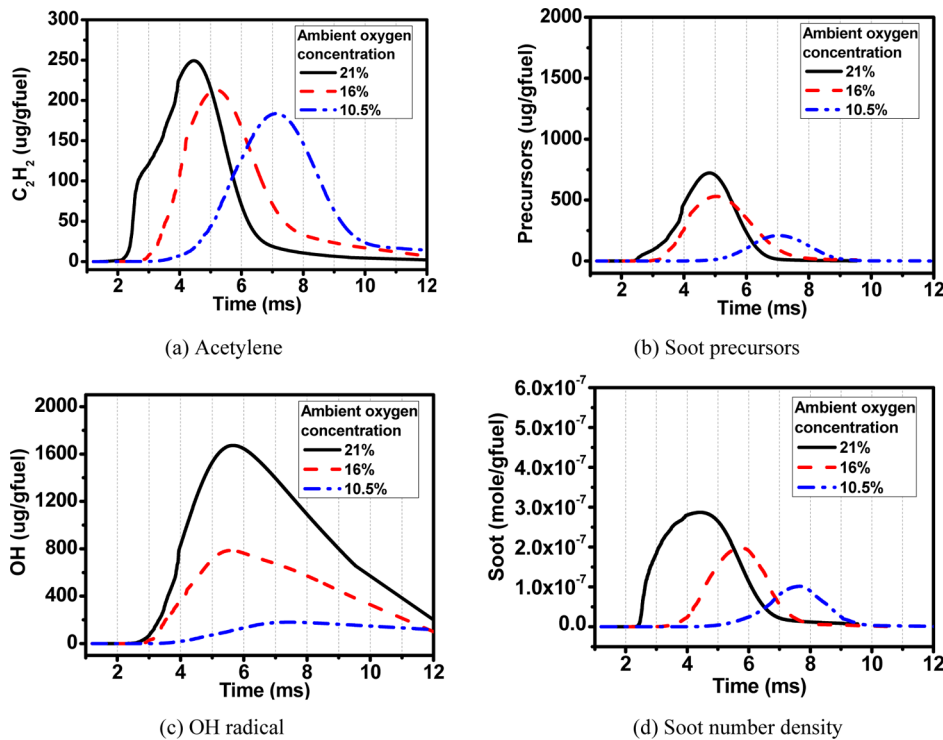


Figure 7. Effects of ambient oxygen concentrations on the concentrations of C_2H_2 , precursors, and OH radical, and soot number density at 800 K.

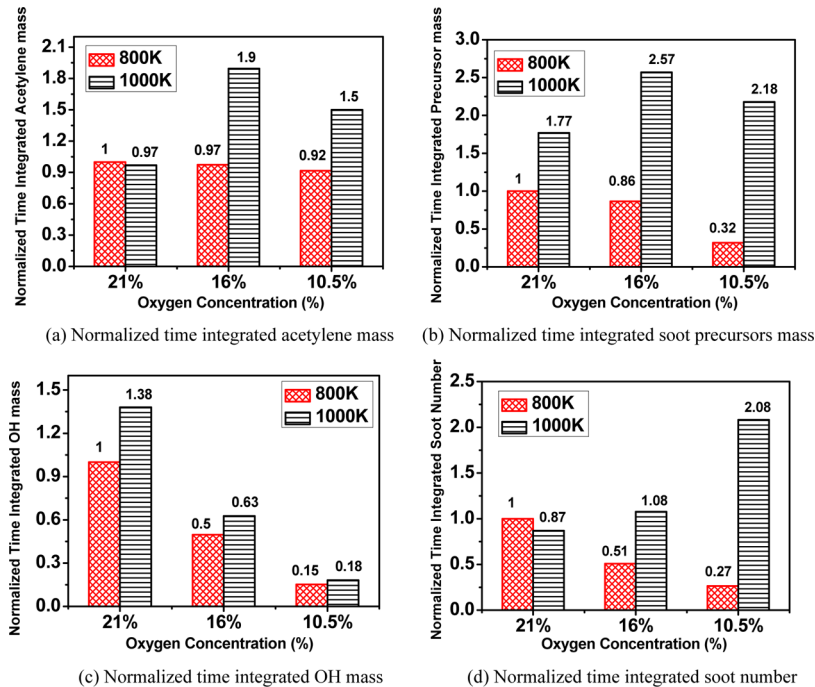


Figure 8. Normalized time-integrated mass of C_2H_2 , soot precursors, OH radical, and the normalized time-integrated soot number under various ambient oxygen concentrations and temperatures.

dominated soot evolution with the drop in initial ambient temperature. As shown in Figures 7 and 8, the reduction amount of soot precursors was larger than that of acetylene with the decrease in ambient temperature, so it can be observed that the formation of soot precursors was more sensitive to temperature than biodiesel pyrolysis. Compared to the NTISM of soot mass, as shown in Figure 5, the time-integrated soot number illustrated a much flatter drop with the decrease of

ambient temperature at a given oxygen concentration, so the mean molecular weight of soot nuclei tended to reduce with decreasing temperature. Since the mean diameter of soot is proportional to the mean molecular weight of soot nuclei, the mean size of soot emissions should be smaller at 800 K.

At 1000 K, both time-integrated soot mass and soot number increased with decreasing ambient oxygen concentrations, but the increase in the amount of time-integrated soot mass was

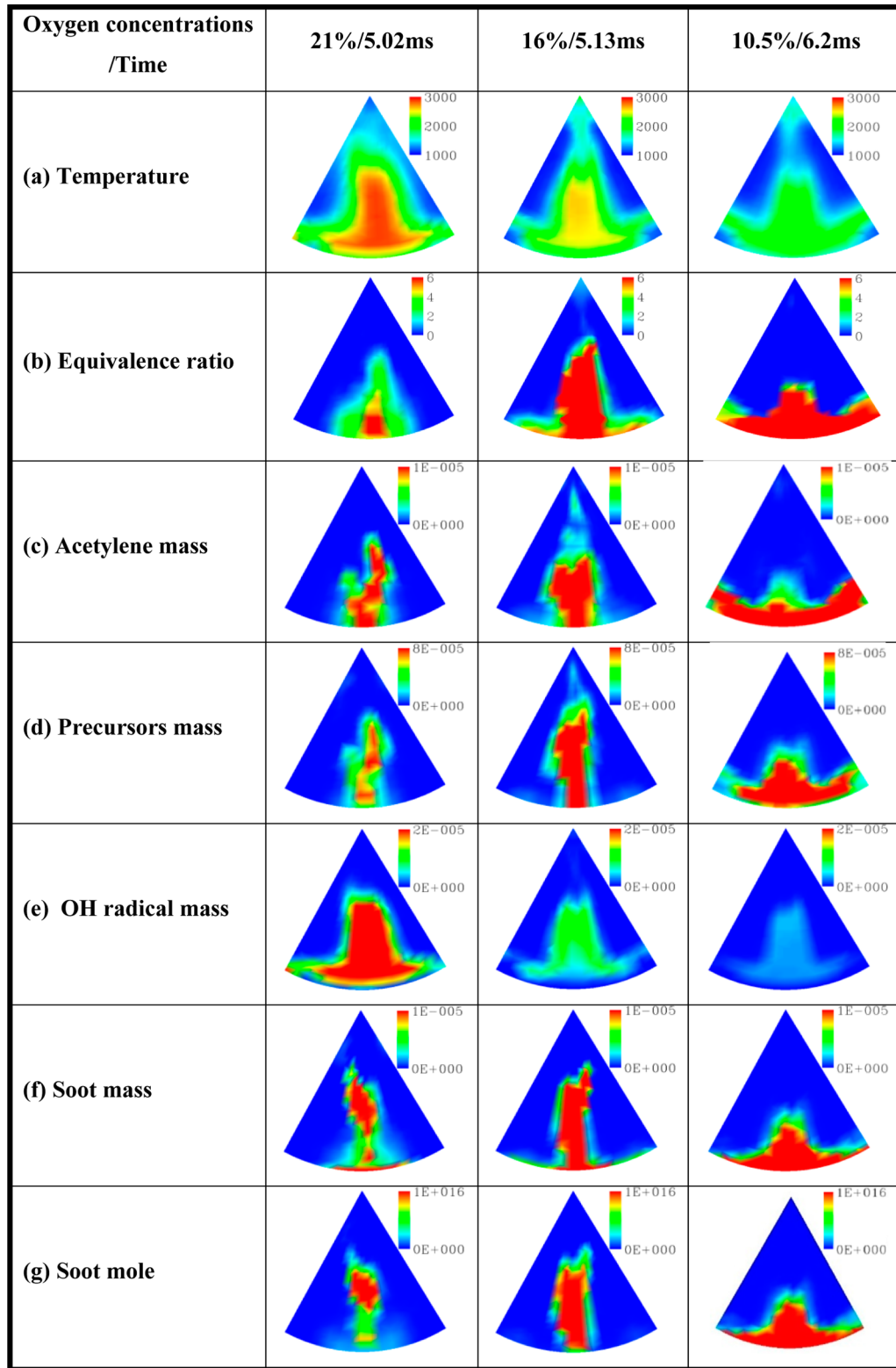


Figure 9. Effects of ambient oxygen concentrations on distributions of temperature, equivalence ratio, and the mass concentrations of acetylene, precursors, OH radical, soot mass, and mole at 1000 K.

larger. Consequently, a growth of mean molecular weight of soot nuclei can be expected and the mean size of soot nuclei should be larger under lower ambient oxygen concentration. As ambient oxygen concentration decreased, the formation of acetylene increased first and then decreased, while the formation of soot precursors showed a monotonous trend,

increasing slightly, as shown in Figure 6. However, for time-integrated mass of soot formation, with regard to relevant species (C_2H_2 and soot precursors), the maximum amount appeared at an ambient oxygen concentration of 16%, because of its longer duration, which should be caused by the higher combustion pressure and heat release rate, as shown in Figure

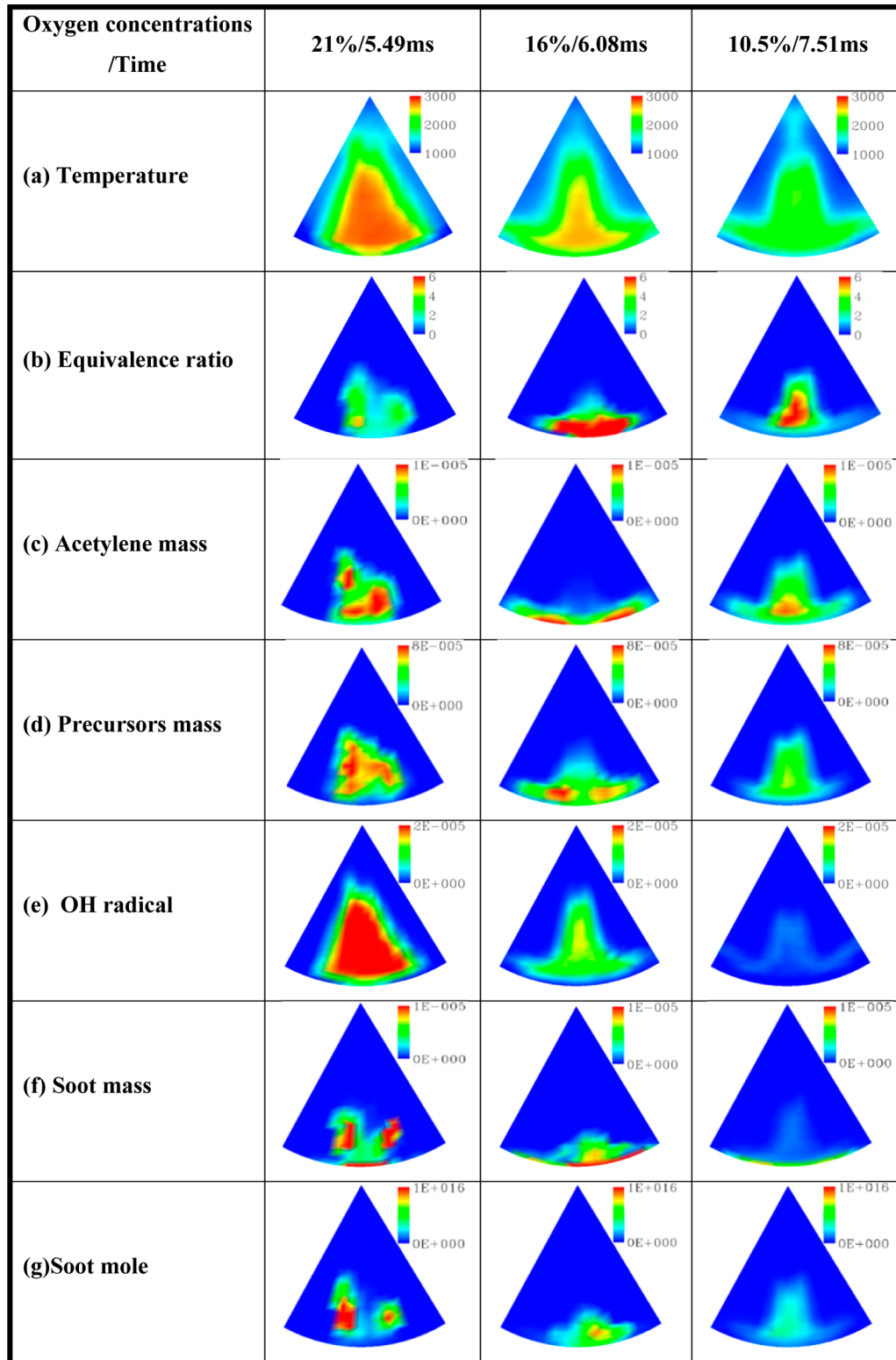


Figure 10. Effects of ambient oxygen concentrations on distributions of temperature, equivalence ratio, and the mass concentrations of acetylene, precursors, OH radical, soot mass, and mole at 800 K.

3. Therefore, the soot formation mechanism under conventional temperature conditions showed a strong dependence on temperature. The time-integrated mass of OH radical, which is a key reactant involved in the soot oxidation mechanism, presented a continuous drop as the ambient oxygen concentration decreased, indicating that the oxidation mecha-

nism continued to be suppressed. At an ambient oxygen concentration of 10.5%, the powerless soot oxidation reactions eliminated soot benefit, because of the weaker formation evidenced by the lower mass concentrations of acetylene and soot precursors, and thus produced a sharp growth in soot mass. Therefore, when heavy EGR is employed to achieve

remarkable suppression on NO_x emissions, the accompanying soot increase is the result of an insufficient soot oxidation mechanism.

In contrast, at a temperature of 800 K, both time-integrated soot mass and soot number decreased with decreasing ambient oxygen concentrations, but the amount of decrease in the time-integrated soot mass was less. Consequently, a growth of mean molecular weight of soot nuclei can be expected and the mean size of soot nuclei should be larger under lower ambient oxygen concentration. As the ambient oxygen concentration was reduced, the time-integrated mass of acetylene, soot precursors, and OH radical presented a continuous drop, so soot formation and oxidation reactions were simultaneously restrained. Finally, the time-integrated soot mass and soot number decreased as the ambient oxygen concentration decreased, because of the dominated suppressed soot formation. As shown in Figure 8, the acetylene only decreased slightly under lower oxygen concentrations, while the soot precursors indicated a more significant reduction tendency than acetylene, which proved to be the bigger contribution of soot precursors in restricting soot formation activities with diluted ambient oxygen.

As the ambient oxygen concentration was reduced, there was an extraordinary decrease in the time-integrated mass of soot oxidation relevant species (i.e., OH radical), regardless of whether the initial ambient temperature was 1000 K or 800 K. However, the time-integrated mass of soot formation relevant species (i.e., acetylene and soot precursors) presented a contrary varying tendency with decreasing ambient oxygen concentrations in conventional and low-temperature conditions. At 800 K, the time-integrated mass of soot formation relevant species decreased with reducing ambient oxygen concentration, while the time-integrated mass of soot formation relevant species at both ambient oxygen concentrations of 16% and 10.5% was larger, compared to that of 21% ambient oxygen concentration at 1000 K. Correspondingly, the nonconsistent behavior of soot nuclei with ambient oxygen dilution in conventional and low-temperature diesel combustion flames was due to the transition in soot formation activities dominated by the combustion temperature.

4.3. Spatial Distributions of Soot Formation/Oxidation Relevant Species. Figures 9 and 10 present the spatial distributions of temperature, equivalence ratio, acetylene, soot precursors, OH radical, soot mass concentrations, and number density under various ambient oxygen concentrations in both conventional and low-temperature conditions. The selected time is the time at which the soot mass concentration reached its peak value. The color bar on the upper right-hand corner presents the range of each simulation parameter. Compared to distributions of acetylene and soot precursors, the OH radical distribution was more similar with temperature distributions. Therefore, the soot oxidation was highly dependent on combustion temperature. It was also clear to see that a high soot number density generally shared the same region where the soot mass concentration was found to be high. When the ambient temperature was reduced from 1000 K to 800 K, the mass distributions of acetylene was almost identical. However, the distributions of soot precursors indicated a lower mass concentration. Unlike the distributions of soot mass and soot number at an initial ambient temperature of 1000 K, the soot reaction zone was mainly condensed downstream of the biodiesel fuel jet and the total area of the soot reaction zone was greatly diminished under low ambient temperature conditions of 800 K.

Regardless of whether the initial temperature was 800 K or 1000 K, the decay in luminosity was observed in the distribution of combustion temperature and OH mass concentration with decreasing ambient oxygen concentration, indicating the lower capability on soot oxidation. Under low oxygen concentration conditions, the combustion temperatures were very similar between ambient temperatures of 800 K and 1000 K, while the distribution of high soot emission was reduced and the total area was greatly diminished at 800 K. The difference in soot distribution can be attributed to the combined effects between the amount of air entrained into spray jet and the ambient oxygen dilution. The lower oxygen concentration resulted in the longer ignition delay, which made more ambient air entrained into the spray jet and produced more regions of low equivalence ratio, and thus the soot formation was suppressed. However, the mixture of fuel/air at the lift-off location became diluted with decreasing oxygen concentration and more inert gas would enter into the spray jet. If the reduction of oxygen concentration can be compensated by more ambient air entrainment, the soot concentration is reduced; otherwise, the amount of soot is increased. At 800 K, the decrease in oxygen concentration was compensated by the greater amount of air entrainment under the longer ignition delay condition; therefore, the equivalence ratio was lower and the soot mass was reduced with reductions in the amount of ambient oxygen. At 1000 K, the difference of ignition delay among the three oxygen concentrations was smaller, in comparison to that observed at 800 K; the decreasing in oxygen concentration was not compensated by more air entrainment. Therefore, the local equivalence ratio and soot formation was obviously increased in the near-wall region, because of the dilution of inert gas.

5. CONCLUSIONS

Experimental and numerical investigations were conducted in this work to analyze the influences of ambient oxygen concentrations (EGR rates) on biodiesel soot behavior in conventional and low-temperature flames. A semiempirical biodiesel soot model was proposed and coupled into a CFD code to analyze the soot evolution process. The primary conclusions are shown as follows:

(1) The proposed semiempirical biodiesel soot model could successfully reproduce the entire process of soot evolution under various oxygen concentrations and ambient temperatures and was an effective tool to analyze the mechanism of soot formation and oxidation.

(2) With the decrease of ambient temperature, the C_2H_2 , soot precursors, OH radical, and soot were reduced, presented later as a threshold of increase, and the time-integrated mass of these species was reduced. The soot formation mechanism dominated soot evolution and caused a lower soot mass with the decrease in ambient temperature. Soot precursors formation presented stronger temperature dependence than biodiesel pyrolysis.

(3) When the ambient temperature is reduced from 1000 K to 800 K, the mass distributions of acetylene was almost identical. However, the distributions of soot precursors indicated a lower mass concentration and the distribution of high equivalence ratio reduced significantly at the low ambient temperature condition. The total soot area and soot concentrations greatly diminished at an ambient temperature of 800 K.

(4) As reducing ambient oxygen concentration, soot formation was inhibited at 800 K, but the soot formation was motivated at 1000 K. The soot oxidation was significant suppressed as ambient oxygen concentration reduced at both 800 and 1000 K. Soot formation transition was the responsible factor for the inconsistent soot behavior, because of the dilution of ambient oxygen in conventional and low-temperature diesel combustion flames.

(5) At 800 K, the decrease in oxygen concentration was compensated by more air entrainment; therefore, the equivalence ratio was lower and soot mass was reduced at lower oxygen concentration. At 1000 K, the reduction of oxygen concentration was not compensated by any more air entrainment; therefore, a higher local equivalence ratio and more soot was observed in the near-wall region at lower oxygen concentrations.

AUTHOR INFORMATION

Corresponding Author

*Tel.: 86-22-27406842, ext. 8011. Fax: 86-22-27383362. E-mail: haifengliu@tju.edu.cn

Notes

The authors declare no competing financial interest.

ACKNOWLEDGMENTS

The authors acknowledged the National Natural Science Foundation of China (NSFC) due to its financial supports on this work by the Project of 51206120.

NOMENCLATURE

A_s = total surface area of a soot particle

CFD = computational fluid dynamics

d_p = mean diameter of the soot nuclei

EGR = exhaust gas recirculation

FILE = forward illumination light extinction

HCCI = homogeneous charge compression ignition

k_B = Boltzmann constant

k_{coa} = collision frequency constant

K_{ext} = extinction coefficient

k_{fm} = collision frequency in the free molecular regime

Kn = Knudsen number

k_{nc} = collision frequency in the near-continuum regime

k_{NSC} = reaction rate constant of the NSC oxidation model

l = gas mean-free path

m_s = soot mass concentration

MW_C = molar weight of a carbon atom

N_s = number density of soot particle

N_A = Avogadro's number

NSC = Nagle–Stickland–Constable oxidation model

p = mean pressure

P = soot precursors

[P] = mole concentration of soot precursors

R = universal gas constant

S = soot nuclei

[S_c] = mole concentration of soot particles

T = mean chamber temperature

y_s = soot mole concentration

Greek Symbols

ρ_s = soot mass density

ω = reaction rate

μ = gas viscosity

REFERENCES

- (1) Lapuerta, M.; Armas, O.; Rodríguez-Fernández, J. Effect of Biodiesel Fuels on Diesel Engine Emissions. *Prog. Energy Combust. Sci.* **2008**, *34*, 198–223.
- (2) Mauss, F.; Schäfer, T.; Bockhorn, H. Inception and Growth of Soot Particles in Dependence on the Surrounding Gas Phase. *Combust. Flame* **1994**, *99*, 697–705.
- (3) Agarwal, A. K. Biofuels (Alcohols and Biodiesel) Applications as Fuels for Internal Combustion Engines. *Prog. Energy Combust. Sci.* **2007**, *33*, 233–271.
- (4) Zhang, J.; Fang, T. Spray Combustion of Biodiesel and Diesel in a Constant Volume Combustion Chamber. *SAE Tech. Pap. Ser.* **2011**, 2011-01-1380.
- (5) Zhang, J.; Jing, W.; Roberts, W. L.; Fang, T. Effects of ambient oxygen concentration on biodiesel and diesel spray combustion under simulated engine conditions. *Energy* **2013**, *57*, 722–732.
- (6) Liu, H. F.; Li, S. J.; Zheng, Z. Q.; Xu, J.; Yao, M. F. Effects of *n*-Butanol, 2-Butanol, and Methyl Octynoate Addition to Diesel Fuel on Combustion and Emissions over a Wide Range of Exhaust Gas Recirculation (EGR) Rates. *Appl. Energy* **2013**, *112*, 246–256.
- (7) Graboski, M. S.; McCormick, R. L. Combustion of Fat and Vegetable Oil Derived Fuels in Diesel Engines. *Prog. Energy Combust. Sci.* **1998**, *24*, 125–164.
- (8) Lee, D.; Choi, S. C.; Lee, C. S. Impact of SME Blended Fuel Combustion on Soot Morphological Characteristics in a Diesel Engine. *Int. J. Automot. Eng.* **2013**, *14*, 757–762.
- (9) Yoon, S. H.; Suh, H. K.; Lee, C. S. Effect of Spray and EGR Rate on the Combustion and Emission Characteristics of Biodiesel Fuel in a Compression Ignition Engine. *Energy Fuels* **2009**, *23*, 1486–1493.
- (10) Qi, D. H.; Geng, L. M.; Chen, H.; Bian, Y. Z.; Liu, J.; Ren, X. C. Experimental Studies of a Naturally Aspirated, DI Diesel Engine Fuelled with Ethanol–Biodiesel–Water Microemulsions. *Renew. Energy* **2009**, *34*, 2706–2713.
- (11) Wang, X. G.; Huang, Z. H.; Kuti, O. A.; Zhang, W.; Nishid, K. An Experimental Investigation on Spray, Ignition and Combustion Characteristics of Biodiesels. *Proc. Combust. Inst.* **2011**, *33*, 2071–2077.
- (12) Qi, D. H.; Leick, M.; Liu, Y.; Lee, C. F. Effect of EGR and Injection Timing on Combustion and Emission Characteristics of Split Injection Strategy DI-Diesel Engine Fueled with Biodiesel. *Fuel* **2011**, *90*, 1884–1891.
- (13) Boehman, A. L.; Song, J.; Alam, M. Impact of Biodiesel Blending on Diesel Soot and the Regeneration of Particulate Filters. *Energy Fuels* **2005**, *19*, 1857–1864.
- (14) Chen, P.; Wang, W.; Roberts, W. L.; Fang, T. Spray and Atomization of Diesel Fuel and its Alternatives from a Single-hole Injector Using a Common Rail Fuel Injection System. *Fuel* **2013**, *103*, 850–861.
- (15) Fang, T.; Lee, C. F. Bio-diesel Effects on Combustion Processes in an HSDI Diesel Engine Using Advanced Injection Strategies. *Proc. Combust. Inst.* **2009**, *32*, 2785–2792.
- (16) Zhang, J.; Jing, W.; Roberts, W. L.; Fang, T. Soot Temperature and *KL* Factor for Biodiesel and Diesel Spray Combustion in a Constant Volume Combustion Chamber. *Appl. Energy* **2013**, *107*, 52–65.
- (17) Wang, X.; Cheung, C. S.; Di, Y.; Huang, Z. Diesel Engine Gaseous and Particle Emissions Fueled with Diesel–Oxygenate Blends. *Fuel* **2012**, *94*, 317–323.
- (18) Wang, X. G.; Kuti, O. A.; Zhang, W.; Nishid, K.; Huang, Z. H. Effect of Injection Pressure on Flame and Soot Characteristics of the Biodiesel Fuel Spray. *Combust. Sci. Technol.* **2010**, *182*, 1369–1390.
- (19) Wang, X. G.; Zheng, B.; Huang, Z. H.; Zhang, N.; Zhang, Y. J.; Hu, E. J. Performance and Emissions of a Turbocharged, High-pressure Common Rail Diesel Engine Operating on Biodiesel/Diesel Blends. *Proc. Inst. Mech. Eng., Part D: J. Auto. Eng.* **2011**, *225*, 127–139.
- (20) Lee, C. S.; Park, S. W.; Kwon, S. I. An Experimental Study on the Atomization and Combustion Characteristics of Biodiesel-Blended Fuels. *Energy Fuels* **2005**, *19*, 2201–2208.

- (21) Szybist, J. P.; Song, J.; Alam, M.; Boehman, A. L. Biodiesel Combustion, Emissions and Emission Control. *Fuel Process. Technol.* **2007**, *88*, 679–691.
- (22) Ye, P.; Boehman, A. L. An Investigation of the Impact of Injection Strategy and Biodiesel on Engine NO_x and Particulate Matter Emissions with a Common-rail Turbocharged DI Diesel Engine. *Fuel* **2012**, *97*, 476–488.
- (23) Ye, P.; Boehman, A. L. Investigation of the Impact of Engine Injection Strategy on the Biodiesel NO_x Effect with a Common-rail Turbocharged Direct Injection Diesel Engine. *Energy Fuels* **2010**, *24*, 4215–4225.
- (24) Palash, S. M.; Kalam, M. A.; Masjuki, H. H.; Masum, B. M.; Fattah, I. M. R.; Mofijur, M. Impacts of Biodiesel Combustion on NO_x Emissions and Their Reduction Approaches. *Renew. Sust. Energy Rev.* **2013**, *23*, 473–490.
- (25) Yoon, S. H.; Suh, H. K.; Lee, C. S. Effect of Spray and EGR Rate on the Combustion and Emission Characteristics of Biodiesel Fuel in a Compression Ignition Engine. *Energy Fuels* **2009**, *23*, 1486–1493.
- (26) Tsolakis, A.; Megaritis, A.; Wyszynski, M. L.; Theinnoi, K. Application of Exhaust Gas Fuel Reforming in Diesel and Homogeneous Charge Compression Ignition (HCCI) Engines Fuelled with Biofuels. *Energy* **2007**, *32*, 2072–2080.
- (27) Song, H.; Tompkins, B. T.; Bittle, J. A.; Jacobs, T. J. Comparisons of NO Emissions and Soot Concentrations from Biodiesel-Fuelled Diesel Engine. *Fuel* **2012**, *96*, 446–453.
- (28) Agarwal, D.; Sinha, S.; Agarwal, A. K. Experimental Investigation of Control of NO_x Emissions in Biodiesel-Fueled Compression Ignition Engine. *Renew. Energy* **2006**, *31*, 2356–2369.
- (29) Fisher, E. M.; Pitz, W. J.; Curran, H. J.; Westbrook, C. K. Detailed Chemical Kinetic Mechanisms for Combustion of Oxygenated Fuels. *Symp. (Int.) Combust.* **2000**, *28*, 1579–1586.
- (30) Dayma, G.; Gail, S.; Dagaut, P. Experimental and Kinetic Modeling Study of the Oxidation of Methyl Hexanoate. *Energy Fuels* **2008**, *22*, 1469–1479.
- (31) Herbinet, O.; Pitz, W. J.; Westbrook, C. K. Detailed chemical kinetic mechanism for the oxidation of biodiesel fuels blend surrogate. *Combust. Flame* **2010**, *157*, 893–908.
- (32) Herbinet, O.; Biet, J.; Hakka, M. H.; Warth, V.; Glaude, P. A.; Nicolle, A.; Battin-Leclerc, F. Modeling Study of the Low-temperature Oxidation of Large Methyl Esters from C₁₁ to C₁₉. *Proc. Combust. Inst.* **2011**, *33*, 391–398.
- (33) Hiroyasu, H.; Kadota, T.; Arai, M. Development and Use of a Spray Combustion Modelling to Predict Diesel Engine Efficiency and Pollutant Emissions. *Bull. JSME* **1983**, *26*, 569–575.
- (34) Karataş, A. E.; Gülder, O. L. Soot Formation in High Pressure Laminar Diffusion Flames. *Prog. Energy Combust. Sci.* **2012**, *38*, 818–845.
- (35) Fusco, A.; Knox-Kelecy, A. L.; Foster, D. E. Application of a Phenomenological Soot Model to Diesel Engine Combustion. In *3rd International Symposium, COMODIA 94*, Yokohama, Japan, 1994; pp 571–576.
- (36) Tao, F.; Reitz, R. D.; Foster, D. E.; Liu, Y. Nine-step Phenomenological Diesel Soot Model Validated over a Wide Range of Engine Conditions. *Int. J. Therm. Sci.* **2009**, *48*, 1223–1234.
- (37) Jia, M.; Xie, M. Z.; Wang, T. Y.; Peng, Z. J. The Effect of Injection Timing and Intake Valve Close Timing on Performance and Emissions of Diesel PCCI Engine with a Full Engine Cycle CFD Simulation. *Appl. Energy* **2011**, *88*, 2967–2975.
- (38) Nerva, J.-E.; Genzale, C. L.; Kook, S.; Garcia-Olivier, J. M.; Pickett, L. M. Fundamental Spray and Combustion Measurements of Soy Methyl-ester Biodiesel. *Int. J. Engine Res.* **2013**, *14*, 373–390.
- (39) Xu, Y.; Lee, C. F. Forward-illumination Light-extinction Technique for Soot Measurement. *Appl. Opt.* **2006**, *45*, 2046–2057.
- (40) Liu, H. F.; Bi, X. J.; Huo, M.; Lee, C. F.; Yao, M. F. Soot Emissions of Various Oxygenated Biofuels in Conventional Diesel Combustion and Low-temperature Combustion Conditions. *Energy Fuels* **2012**, *26*, 1900–1911.
- (41) Liu, H. F.; Lee, C. F.; Huo, M.; Yao, M. F. Combustion Characteristics and Soot Distributions of Neat Butanol and Neat Soybean Biodiesel. *Energy Fuels* **2011**, *25*, 3192–3203.
- (42) Liu, H. F.; Lee, C. F.; Huo, M.; Yao, M. F. Comparison of Ethanol and Butanol as Additives in Soybean Biodiesel Using a Constant Volume Combustion Chamber. *Energy Fuels* **2011**, *25*, 1837–1846.
- (43) Xu, Y.; Lee, C. F. Investigation of Soot Formation in Diesel Combustion Using Forward Illumination Light Extinction (FILE) Technique. *SAE Tech. Pap. Ser.* **2004**, 2004-01-1411.
- (44) Xu, Y.; Lee, C. F. Investigation of Fuel Effects on Soot Formation Using Forward Illumination Light Extinction (FILE) Technique. *SAE Tech. Pap. Ser.* **2005**, 2005-01-0365.
- (45) Xu, Y.; Lee, C. F. Study of Soot Formation of Oxygenated Diesel Fuels Using Forward Illumination Light Extinction (FILE) Technique. *SAE Tech. Pap. Ser.* **2006**, 2006-01-1415.
- (46) Buchholz, B. A.; Mueller, C. J.; Upatnieks, A.; Martin, G. C.; Pitz, W. J.; Westbrook, C. K. Using Carbon-14 Isotope Tracing to Investigate Molecular Structure Effects of the Oxygenate Dibutyl Maleate on Soot Emissions from a DI Diesel Engine. *SAE Tech. Pap. Ser.* **2004**, 2004-01-1849.
- (47) Kohse-Höinghaus, K.; Oßwald, P.; Cool, T. A.; Kasper, T.; Hansen, N.; Qi, F.; Westbrook, C. K.; Westmoreland, P. R. Biofuel Combustion Chemistry: from Ethanol to Biodiesel. *Angew. Chem., Int. Ed.* **2010**, *49*, 3572–3597.
- (48) Szybist, J. P.; Boehman, A. L.; Haworth, D. C.; Koga, H. Premixed Ignition Behavior of Alternative Diesel Fuel-relevant Compounds in a Motored Engine Experiment. *Combust. Flame* **2007**, *149*, 112–128.
- (49) Dagaut, P.; Gail, S.; Sahasrabudhe, M. Rapeseed Oil Methyl Ester Oxidation over Extended Ranges of Pressure, Temperature, and Equivalence Ratio: Experimental and Modeling Kinetic Study. *Proc. Combust. Inst.* **2007**, *31*, 2955–2961.
- (50) Lai, J. Y. W.; Lin, K. C.; Violi, A. Biodiesel Combustion: Advances in Chemical Kinetic Modeling. *Prog. Energy Combust. Sci.* **2011**, *37*, 1–14.
- (51) Good, D. A.; Francisco, J. S. Tropospheric Oxidation Mechanism of Dimethyl Ether and Methyl Formate. *J. Phys. Chem. A* **2000**, *104*, 1171–1185.
- (52) Melius, C. F.; Colvin, M. E.; Marinov, N. M.; Pitz, W. J.; Senkan, S. M. *Proc. Combust. Inst.* **1996**, *26*, 685–692.
- (53) Wang, H.; Frenklach, M. A. *Combust. Flame* **1997**, *110*, 173–221.
- (54) Schuetz, C. A.; Frenklach, M. *Proc. Combust. Inst.* **2002**, *29*, 2307–2314.
- (55) Skjøth-Rasmussen, M. S.; Glarborg, P.; Ostberg, M.; Johannessen, J. T.; Livbjerg, H.; Jensen, A. D. *Combust. Flame* **2004**, *136*, 91–128.
- (56) Wang, H.; Reitz, R. D.; Yao, M.; Yang, B.; Jiao, Q.; Qiu, L. *Combust. Flame* **2013**, *160*, 504–519.
- (57) Keller, A.; Kovacs, R.; Homann, K. H. *Phys. Chem. Chem. Phys.* **2000**, *2*, 1667–1675.
- (58) Mathieu, O.; Frache, G.; Djebaili-Chaumeix, N.; Paillard, C. E.; Krier, G.; Muller, J. F. *Proc. Combust. Inst.* **2007**, *31*, 511–519.
- (59) Kazakov, A.; Foster, D. E. Modeling of Soot Formation During DI Diesel Combustion Using a Multi-Step Phenomenological Model. *SAE Tech. Pap. Ser.* **1998**, No. 982463.
- (60) Braun, A.; Huggins, F. E.; Seifert, S.; Ilavsky, J.; Shah, N.; Kelly, K. E.; Sarofim, A.; Huffman, G. P. *Combust. Flame* **2004**, *137*, 63–72.
- (61) di Stasio, S. *J. Aerosol Sci.* **2001**, *32*, 509–524.
- (62) Leung, K. M.; Lindstedt, R. P.; Jones, W. P. *Combust. Flame* **1991**, *87*, 289–305.
- (63) Neoh, K. G.; Howard, J. B.; Sarofim, A. F. *Symp. (Int.) Combust.* **1985**, *20*, 951–957.
- (64) Tree, D. R.; Svensson, K. I. *Prog. Energy Combust. Sci.* **2007**, *33*, 272–309.
- (65) Reitz, R. D.; Diwakar, R. Structure of High-Pressure Fuel Sprays. *SAE Tech. Pap. Ser.* **1987**, No. 870598.
- (66) Liu, A. B.; Reitz, R. D. *Atomization Sprays* **1993**, *3*, 55–75.

- (67) Patterson, M.; Kong, S.; Hampson, G.; Reitz, R. D. *SAE Tech. Pap. Ser.* **1994**, No. 940523SAE.
- (68) Han, Z.; Reitz, R. D. *Combust. Sci. Technol.* **1995**, *106*, 267–295.
- (69) Kong, S.; Han, Z.; Reitz, R. D. The Development and Application of a Diesel Ignition and Combustion Model for Multidimensional Engine Simulation. *SAE Tech. Pap. Ser.* **1995**, No. 950278.
- (70) Peng, Z. J.; Liu, B.; Wang, W. J.; Lu, L. P. *Energies (Basel, Switz.)* **2011**, *4*, 517–531.
- (71) Peng, Z. J.; Jia, M. *Energy Fuels* **2009**, *23*, 5855–5864.